Period-Colour and Amplitude-Colour relations for OGLE-δ Scuti stars in the Galactic Bulge and LMC

Mami Deka,[1]⋆ Shashi M. Kanbur,[2]† Sukanta Deb,[1,3]‡ Susmita Das,[4] Kerdaris Kurbah,[1] Earl P. Bellinger,[5,6] Anupam Bhardwaj[7]

[1]*Department of Physics, Cotton University, Panbazar, Guwahati 781001,Assam, India*
[2]*Department of Physics, State University of New York Oswego, Oswego, NY 13126, USA*
[3]*Space and Astronomy Research Center, Cotton University, Panbazar, Guwahati 781001, Assam, India*
[4]*Konkoly Observatory, CSFK, Konkoly Thege Miklós út 15-17, H-1121, Budapest, Hungary*
[5]*Max Planck Institute for Astrophysics, Garching, Germany*
[6]*Stellar Astrophysics Centre, Aarhus, Denmark*
[7]*INAF-Osservatorio Astronomico di Capodimonte, Via Moiariello 16, I-801301, Napoli, Italy*

ABSTRACT

We present an analysis on the behaviour of the Galactic bulge and the Large Magellanic Cloud (LMC) δ Scuti stars in terms of period-colour and amplitude-colour (PCAC) relations at maximum, mean and minimum light. The publicly available Optical Gravitational Lensing Experiment-IV (OGLE-IV) light curves for Galactic bulge and OGLE-III light curves for LMC δ Scuti stars are exploited for the analysis. It has been found that the Galactic bulge δ Scuti stars obey flat PC relations at *maximum/mean/minimum* light while the LMC δ Scutis have *sloped/sloped/flat* PC relations at *maximum/mean/minimum* light. Both the Galactic bulge and the LMC δ Scutis have *sloped/flat/sloped* AC relations at *maximum/mean/minimum*. These relations also show that Galactic δ Scutis are hotter as compared to their LMC counterparts. The period-amplitude (PA) relations for δ Scutis exhibit different behaviour in the Galactic bulge and the LMC. The LMC variables are found to have higher amplitudes at a given period. The amplitude of the Galactic bulge δ Scuti shows a bimodal distribution which can be modelled using a two-component Gaussian Mixture Model: one component with a lower amplitude and another with a higher amplitude. The observed behaviour of the δ Scuti PCAC relations can be explained using the theory of the interaction of hydrogen ionization front (HIF) and stellar photosphere as well as the PA diagram. We use MESA-RSP to calculate theoretical non-linear hydrodynamical pulsation models for δ Scuti stars with input metallicities of $Z = 0.02$ and $Z = 0.008$ appropriate for the Galactic bulge and LMC, respectively. The observed PCAC relations and theoretical calculations support the HIF-photosphere interaction theory.

Key words: stars: evolution-stars:variables:Delta Scuti-Galaxy:bulge-Magellanic Clouds

1 INTRODUCTION

δ Scutis are pulsating variable and intermediate mass stars with masses in the range $(1.0 - 3.0)\ M_\odot$ having spectral types between A2 and F2 located at the intersection of the Cepheid instability strip with the main sequence (Goupil et al. 2005; Jayasinghe et al. 2020; Bedding et al. 2020). Their pulsation periods lie in the range $(0.03 - 0.3)$ days (Breger 1979). They exhibit a wide range of metallicity and temperature; and pulsate in both single- and multi-modes (Templeton 2000; Murphy et al. 2019). They serve as an important astrophysical tool to test the theories of stellar pulsation and evolution. The single-mode δ Scuti obey a period-luminosity (PL) relation, which make them reliable distance indicators (McNamara 1997; McNamara 2011; Ziaali et al. 2019; Poro et al. 2021), while multi-mode δ Scuti stars can be used to understand the properties of deep stellar interiors (Breger & Pamyatnykh 1998).

δ Scuti stars can be divided into various subclasses based on their metallicities, light curve shapes and amplitudes. On the basis of metallicity, they can be classified into Population-I δ Scuti stars (metal rich), and Population-II SX Phoenicis stars (metal poor). However, not all the SX Phoenicis are found to be metal poor (Nemec et al. 2017). A clear distinction between these two populations of δ Scuti stars is yet not possible and they may therefore be considered as stars having mixed populations (Nemec et al. 2017; Guzik 2021). Further, based on their pulsation behaviour, they are divided into two classes: high amplitude δ Scuti stars (HADS-) and low amplitude δ Scuti stars (LADS). HADS can be found in the post main-sequence region of the instability strip, while low amplitude δ Scuti stars are located in all regions of the δ Scuti instability strip (Templeton 2000; Chang et al. 2013).

The period-colour and amplitude-colour (PCAC) relations have been used extensively to study the radiation hydrodynamics of outer envelope structure and evolutionary status of Cepheids and RR Lyraes (Simon et al. 1993; Kanbur & Ngeow 2004; Bhardwaj et al. 2014; Ngeow et al. 2017; Das et al. 2018). These

⋆ E-mail:mamideka8@gmail.com
† E-mail:shashi.kanbur@oswego.edu
‡ E-mail: sukanta.deb@cottonuniversity.ac.in

studies have found that the PCAC relations of different types of pulsating stars show different behaviour at maximum/mean/minimum light; long period ($P > 10$ days) Classical Cepheids exhibit flat/sloped PC relations at maximum/minimum light, while RR Lyraes show sloped/flat PC relations at maximum/minimum light (Kanbur & Ngeow 2004; Bhardwaj et al. 2014, and references therein). Das et al. (2020) extended this further to include Type II Cepheids. They found that the contrasting behaviour of the PCAC relations are strongly correlated with the relative location of HIF and stellar photosphere. The photosphere is considered being at optical depth $\tau = \frac{2}{3}$, and the HIF is defined to be the region where the majority of hydrogen becomes ionized. The stellar photosphere and HIF are not always co-moving during a pulsation cycle. The HIF moves "in and out" within the mass distribution during a pulsation cycle. Besides, the relative location of the HIF and the stellar photosphere is pulsation-phase dependent. The HIF interacts with the photosphere at those phases where the photosphere lies at the base of HIF. This has been well-established in the literature (Simon et al. 1993; Kanbur 1995; Kanbur & Hendry 1996; Kanbur & Ngeow 2004; Bhardwaj et al. 2014; Ngeow et al. 2017; Das et al. 2018, 2020).

The PCAC relations as a function of phase are important probes of the structure of the outer envelope and offer an insight into the physics of stellar pulsation and evolution (Simon et al. 1993; Kanbur 1995). They also influence the period-luminosity (PL) relations which is crucial for the distance scale and non-cosmic microwave background estimates of Hubble's constant (Beaton et al. 2016; Riess et al. 2016, 2019). Changes in the behaviour of the PC relation can be reflected on the PL relation through the PLC relation as PC/PL relations are just the projection of the PLC (period-luminosity-colour) relation on either the PC or PL (period-magnitude) planes. Since the PLC/PL/PC relations at mean light are the average of the corresponding relations through pulsation phase, changes in these relations at a particular phase or range of phases can be reflected in changes in the relations at mean light. For example, Das et al. (2020, and references therein) showed evidence of the nonlinear PC relation for LMC Cepheids at certain phases. This leads to a nonlinear PL relation at those phases (Bhardwaj et al. 2016). This effect is reduced at mean light. The theory initiated in Simon, Kanbur & Mihalas (1993) and developed in Das et al. (2020, and references therein) demonstrate how the interaction of the stellar photosphere and HIF can produce such changes in the multiphase PC relation.

In this study, we have investigated the observed PCAC relations at maximum/mean/minimum light of δ Scuti stars for the first time and verifies the HIF-photosphere interaction theory of Simon, Kanbur & Mihalas (1993) using MESA-RSP code.

The remaining paper is organized as follows: In Section 2, the selection and cleaning criteria of data is discussed. The methods and analysis criteria are discussed in Section 3. Section 4 describes the results of this work. Finally, we summarize the results of the work in Section 6.

2 SELECTION AND CLEANING OF DATA

The optical (V, I)-band photometric data and light curves of δ Scuti stars belonging to the Galactic bulge are taken from the OGLE-IV database (Soszyński et al. 2021) and those for the LMC from the OGLE-III database (Poleski et al. 2010). At first, possible contaminant sources (foreground and background stars) are separated from the Galactic bulge stars and then removed using a colour-magnitude diagram (CMD). The CMD is constructed using the mean appar-

ent (V, I)-band magnitudes as given in the database by closely following Pietrukowicz et al. (2015). Secondly, the uncertain stars as listed in the 'remarks.txt' file provided by OGLE-IV (for the Galactic bulge) and OGLE-III (for the LMC) databases are removed. From this cleaned sample, finally, we choose well-sampled light curves of mono-periodic δ Scuti stars with more than 30 data points for the analysis. The number of common stars in the final sample with complementary photometric data available in both the I- and V-bands for the Galactic bulge and LMC are 3202 and 1102, respectively.

3 METHODS

The Fourier decomposition method is used to obtain the light curve parameters for the present study. Since the method can lead to numerical ringing when the raw data contains extreme outliers, the removal of these outliers from the raw light curve data is extremely important. The outliers are removed from the raw light curves using the following condition (Leys et al. 2013):

$$\frac{|m - \text{Median}(m)|}{\text{MAD}(m)} \geq 3.0,$$

where m is the observed magnitude, MAD represents the median absolute deviation. After carrying out extreme outlier removal steps on the raw light curves, the Fourier decomposition method is used to obtain the V- and I-band light curve parameters of the sample of δ Scuti stars. The light curves are fitted with a Fourier sine series of the form (Deb & Singh 2009) employing 3σ outlier clipping:

$$m(t) = A_0 + \sum_{i=1}^{N} A_i \sin[i\omega(t_i - t_0) + \phi_i], \tag{1}$$

where A_0 represents mean magnitude, $\omega = \frac{2\pi}{P}$ is the angular frequency, and P and t_i denote the period of a star in days and the times of observations, respectively. The values of P and t_0 are taken as given in the database. Here t_0 represents the epoch of maximum light for the V- band which corresponds to maximum light at phase zero. The components A_i and ϕ_i denote the ith order Fourier coefficients, and N is the order of the fit. The value of N is taken to be 3 and 4 for LMC and Galactic bulge, respectively. Examples of Fourier fitted light curves are displayed in Fig. 1 and Fig. 2. Equation (1) has $2N + 1$ unknown parameters. The light curves are phased using

$$\Phi_i = \frac{t_i - t_0}{P} - \text{Int}\left(\frac{t_i - t_0}{P}\right). \tag{2}$$

From the Fourier fitted-light curve, the colours at maximum, mean and minimum light are obtained as follows:

$$(V - I)_{\text{max}} = V_{\text{max}} - I_{\text{phmax}} \tag{3}$$

$$(V - I)_{\text{mean}} = V_{\text{mean}} - I_{\text{mean}} \tag{4}$$

$$(V - I)_{\text{min}} = V_{\text{min}} - I_{\text{phmin}} \tag{5}$$

where $V_{\text{max}}, V_{\text{mean}}$ and V_{min} denote the maximum, mean and minimum magnitudes in the V-band while $I_{\text{phmax}}, I_{\text{phmin}}$ correspond to I-band magnitudes at the same phase of V_{max} and V_{min}, respectively. Here I_{mean} is the mean I-band magnitude. This way of defining colours at maximum/minimum light allows for phase discrepancies between different bands.

To correct apparent magnitude values in the V- and I-band for the δ Scuti stars of the Galactic bulge, we use the Nataf et al. (2013) extinction calculator, which is appropriate for the bulge. For a given pair of (l, b) values, the calculator returns the extinction value in the I-band A_I as well as the colour excess $E(V - I)$. Using these two values, the extinction in the V-band A_V is calculated. The Nataf et al.
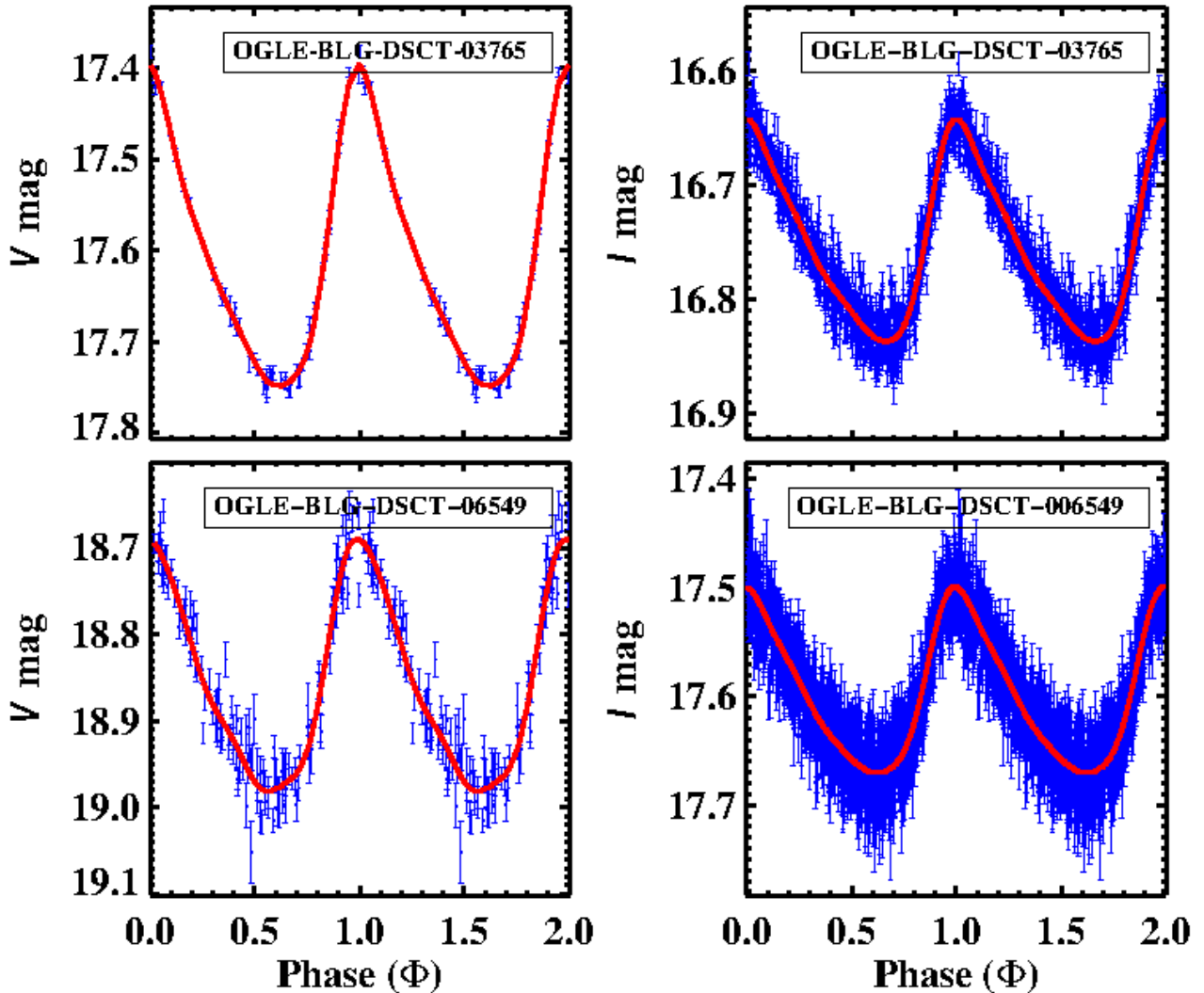
Figure 1. Two randomly selected light curves of Galactic bulge δ Scuti stars in V- and I- band. The red solid line represents the Fourier fitted curve.

(2013) calculator is based on $E(J - K_S)$ reddening values from Gonzalez et al. (2012). Due to the non-standard nature of the reddening law towards the Galactic bulge (Popowski 2000; Udalski 2003; Nishiyama et al. 2009; Nataf et al. 2013; Matsunaga et al. 2013), the A_V and A_I values have also been calculated adopting the standard Cardelli et al. (1989) reddening law and $E(J - K_S)$ values from Gonzalez et al. (2012) reddening map ($\frac{A_I}{A_V} = 0.26$; $\frac{A_I}{A_V} = 0.479$).

To correct for extinction in the LMC, $E(V - I)$ is obtained from the Haschke et al. (2011) reddening map which is converted into $E(B - V)$ values using $E(B - V) = \frac{E(V-I)}{1.38}$ (Tammann et al. 2003). The extinction values are obtained using Cardelli et al. (1989) reddening law: $A_V = 3.32E(B - V)$ and $A_I = 1.94E(B - V)$ (Schlegel et al. 1998). The $E(V - I)$ values for the LMC are also obtained from the most accurate optical reddening map of Skowron et al. (2021) for the Magellanic Clouds. The extinctions A_I and A_V are obtained using the relations $A_I = 1.5E(V-I)$ and $A_V = 2.5E(V-I)$ (Skowron et al. 2021).

Once the magnitudes and the colours of the δ Scuti stars are corrected for extinction and reddening, we fit linear regression models to the PCAC relations employing an iterative 3σ outlier clipping. The results obtained from these analyses are discussed in the following section.

4 ANALYSIS AND RESULTS

4.1 PCAC relations

Simon, Kanbur & Mihalas (1993) established that the PCAC relation at maximum and minimum light for Cepheids can be used to explore the radiation hydrodynamics of the star's outer envelope. They also explained the flat and sloped PC relations of Galactic Cepheids at maximum and minimum light, respectively, using the HIF-photosphere interaction theory. This theory has been verified based on the PCAC relations obtained using different types of pulsat-
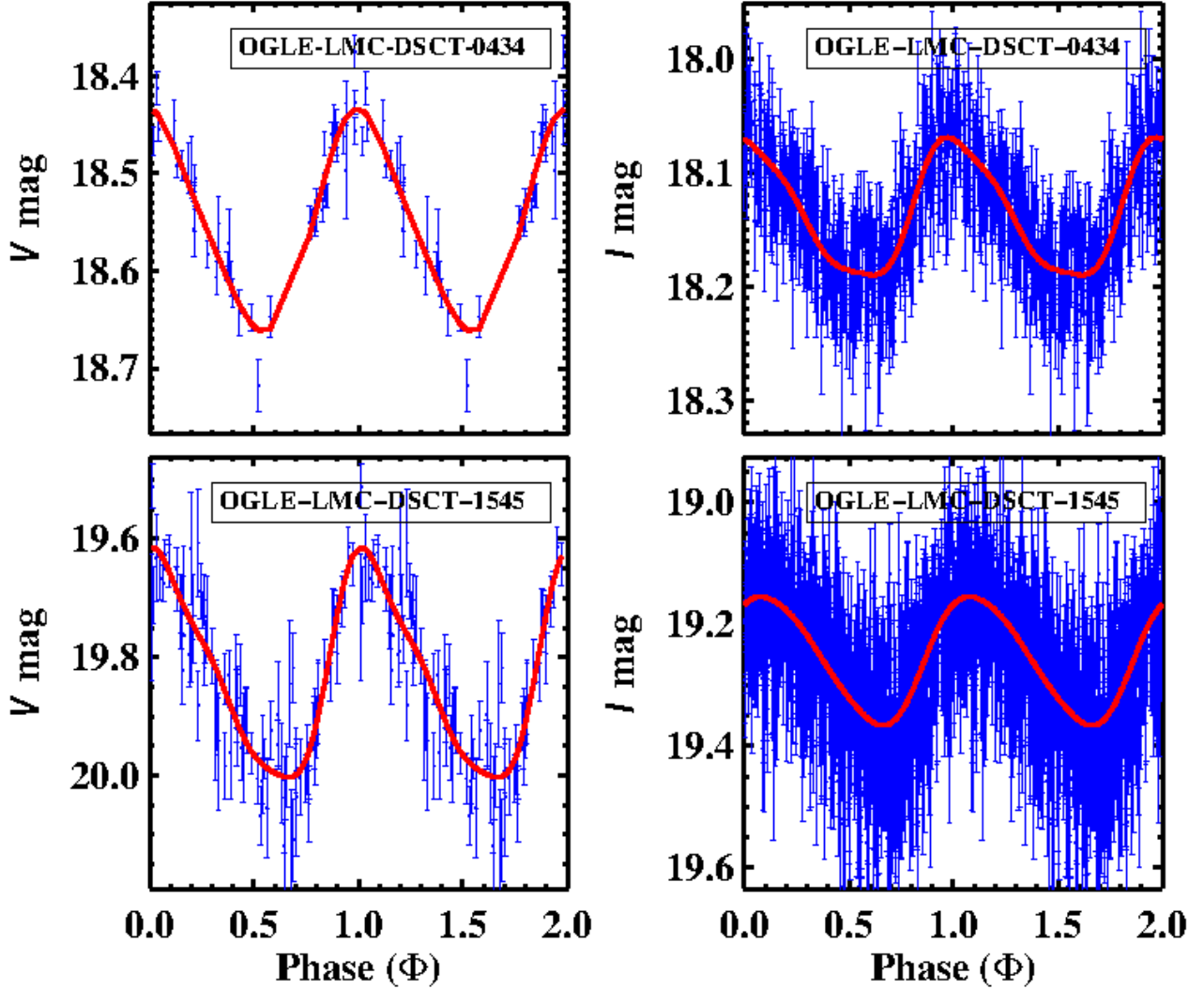
Figure 2. Same as Fig. 1 for LMC.

ing stars (Bhardwaj et al. 2014; Ngeow et al. 2017; Das et al. 2018, 2020, and references therein). Here, we extend it to δ Scuti stars for the first time using the latest OGLE data available for the Galactic bulge and the LMC. The PCAC and PA plots for the Galactic bulge and the LMC δ Scuti stars are shown in Fig. 3 and 6, respectively. The results obtained from the PCAC and PA analyses are summarized in Tables 1 and 2, respectively.

4.1.1 Galactic Bulge δ Scuti

The left panel of Fig. 3 shows the PCAC at maximum/mean/minimum light for the Galactic bulge δ Scuti stars. The parameters of the fitted relations are provided in Table 1. The Galactic PC slopes at max/mean/min light are statistically close to zero. We observe significantly negative/positive AC slope at maximum/minimum light while the slopes of AC relations are flat at mean light.

4.1.2 LMC δ Scuti

The right panel of Fig. 3 shows the PCAC plots at maximum/mean/minimum light for the LMC δ Scuti stars. The solid line in black colour represents the fitted relations with the parameters as provided in Table 1. We find sloped PC relations at maximum/mean light and a flat relation at minimum light. Furthermore, the AC relation is sloped at maximum/minimum light while flat at mean light. The LMC δ Scuti stars are found to exhibit similar behaviour as displayed by the RRab stars when compared with the results obtained by Das et al. (2020). These results are independent of reddening maps.

It is evident from Table 1 that the intercepts of PC relations at maximum/mean/minimum light of Galactic bulge stars have numerically smaller values than those for the LMC stars. A colour difference of $V - I \approx -0.20$ mag at mean light between the Galactic and LMC δ Scutis indicates that the Galactic δ Scutis are comparatively hotter than their LMC counterparts.

The dispersions in the PCAC relations of δ Scuti stars are simi-

Table 1. The slopes and intercepts of PCAC relation for Galactic bulge and LMC δ Scuti stars within 3σ uncertainty.

	Phase	Slope	Intercept	σ^{a}	Nature of slope	F^{b}	$P(F)^{c}$	R^{2d}
		Galactic bulge (Using reddening law from Nataf et al. 2013)						
PC	Max	0.002 ± 0.017	0.228 ± 0.019	0.132	Flat	0.010	0.920	0.000
	Mean	0.054 ± 0.016	0.374 ± 0.019	0.126	Flat	10.519	0.000	0.003
	Min	0.085 ± 0.018	0.467 ± 0.020	0.133	Flat	22.696	0.000	0.007
AC	Max	-0.257 ± 0.014	0.308 ± 0.004	0.122	Sloped	352.500	0.000	0.103
	Mean	0.024 ± 0.014	0.304 ± 0.005	0.127	Flat	3.862	0.082	0.001
	Min	0.161 ± 0.014	0.320 ± 0.005	0.132	Sloped	117.331	0.000	0.037
		Galactic bulge (Using reddening law from Cardelli et al. 1989)						
PC	Max	-0.055 ± 0.023	0.053 ± 0.026	0.171	Flat	8.257	0.004	0.002
	Mean	-0.020 ± 0.022	0.181 ± 0.025	0.167	Flat	1.549	0.213	0.001
	Min	-0.000 ± 0.023	0.265 ± 0.026	0.168	Flat	0.012	0.912	0.000
AC	Max	-0.309 ± 0.016	0.216 ± 0.006	0.163	Sloped	316.274	0.000	0.093
	Mean	-0.024 ± 0.018	0.212 ± 0.006	0.167	Flat	2.844	0.092	0.001
	Min	0.122 ± 0.019	0.226 ± 0.007	0.168	Sloped	32.186	0.000	0.010
		LMC (Using reddening map from Haschke et al. 2011)						
PC	Max	0.328 ± 0.022	0.616 ± 0.022	0.098	Sloped	223.824	0.000	0.177
	Mean	0.191 ± 0.021	0.598 ± 0.021	0.093	Sloped	82.922	0.000	0.074
	Min	0.091 ± 0.026	0.599 ± 0.026	0.119	Flat	11.868	0.001	0.011
AC	Max	-0.325 ± 0.016	0.424 ± 0.008	0.091	Sloped	377.734	0.000	0.268
	Mean	0.014 ± 0.017	0.396 ± 0.008	0.096	Flat	0.733	0.392	0.001
	Min	0.252 ± 0.020	0.394 ± 0.009	0.112	Sloped	152.250	0.000	0.127
		LMC (Using reddening map from Skowron et al. 2021)						
PC	Max	0.318 ± 0.022	0.572 ± 0.022	0.099	Sloped	205.216	0.000	0.164
	Mean	0.186 ± 0.021	0.560 ± 0.021	0.092	Sloped	81.158	0.000	0.072
	Min	0.087 ± 0.026	0.562 ± 0.026	0.119	Flat	10.965	0.000	0.001
AC	Max	-0.342 ± 0.017	0.400 ± 0.008	0.091	Sloped	421.171	0.000	0.290
	Mean	0.002 ± 0.017	0.372 ± 0.008	0.095	Flat	0.008	0.928	0.000
	Min	0.229 ± 0.021	0.373 ± 0.009	0.114	Sloped	123.205	0.000	0.105

[a] Dispersions in the PCAC relations;
[b] Value of F-statistic;
[c] Probability of F-statistic;
[d] Coefficient of variation for each linear regression.

Table 2. The slopes and intercepts of PA relations for Galactic bulge and LMC δ Scuti stars within 3σ uncertainty.

	Slope	Intercept	σ^{e}	R^{2f}	
		Galactic bulge			
V Band	0.756 ± 0.096	1.234 ± 0.121	0.132	0.992	Period < 0.06 d
	0.170 ± 0.032	0.515 ± 0.034	0.158	0.987	Period ≥ 0.06 d
I Band	0.382 ± 0.052	0.632 ± 0.066	0.072	0.997	Period < 0.06 d
	0.112 ± 0.019	0.308 ± 0.020	0.094	0.994	Period ≥ 0.06 d
		LMC			
V Band	-0.569 ± 0.034	-0.149 ± 0.034	0.152	0.393	All period
I Band	-0.311 ± 0.018	-0.077 ± 0.018	0.082	0.476	All period

[e] Dispersions in the PCAC relations;
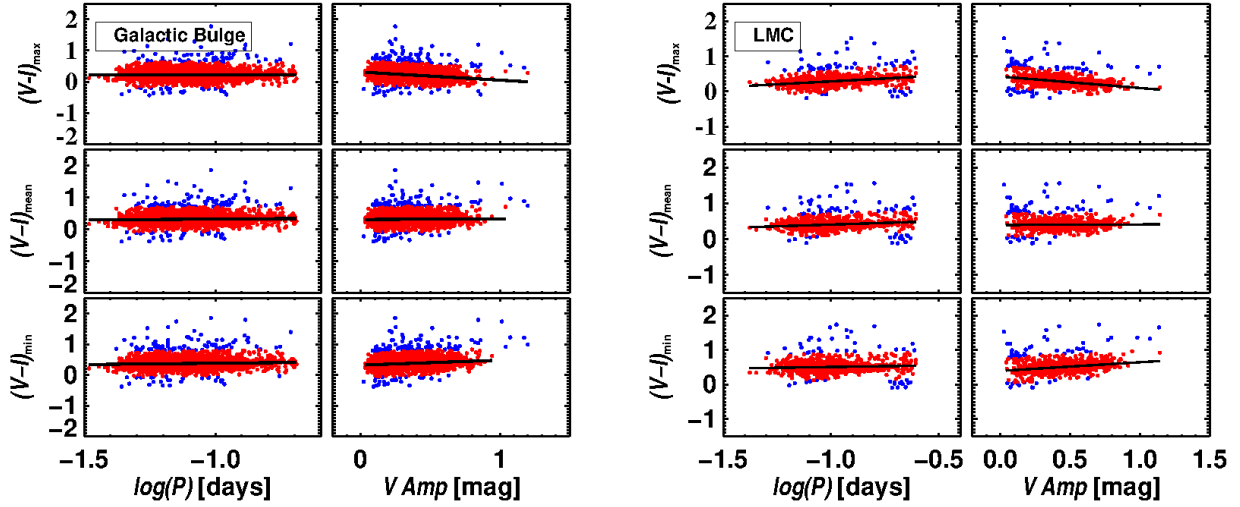[f] Coefficient of variation for each linear regression.

Figure 3. Left panel: PCAC diagram for Galactic bulge single-mode δ Scuti stars (with iterative 3σ outliers clipping). The left/right sides are the PC/AC diagrams at maximum (top), mean (middle) and minimum (bottom). The outliers are shown by the blue points. The solid lines represent the best fit to the plots. Right panel: Same for the LMC.
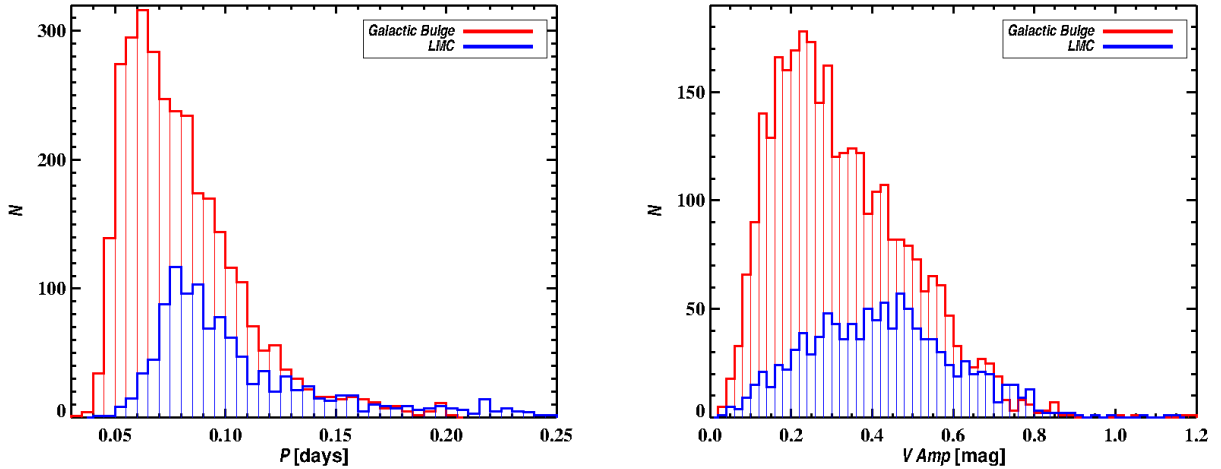

Figure 4. Left panel: Histogram of period distributions of δ Scuti stars for both Galactic bulge (red) and LMC (blue). Right panel: Histogram of amplitude distributions of δ Scuti stars for both Galactic bulge (red) and LMC (blue).

lar to those of RR Lyraes (Bhardwaj et al. 2014) and BL Her stars (Das et al. 2020). To see whether the large dispersions are effecting the linear PCAC relations of δ Scuti stars or not, we made some further tests. We calculate the coefficient of variation R^2 for each linear regression as follows:

$$R^2 = 1 - \frac{\sum (y_i - \hat{y}_i)}{\sum (y_i - \overline{y})}. \tag{6}$$

Here y_i represents the observed reddening corrected colours of the stars, $\hat{y}_i$, the estimated values of y_i form the linear relations and $\overline{y}$ is the mean value of y_i. The obtained values of R^2 are listed in Tables 1 and 2. The value of R^2 is close to zero for the Galactic bulge PC relations at all the phases, as expected. However, the intercepts of the Galactic PC relations at maximum and minimum light are statistically significantly different from each other. This is to be expected as the photosphere would be hotter at maximum light. For the LMC

PC relations, $R^2 \approx 0$ at minimum light, which supports the flat relation obtained, while $R^2 > 0$ at maximum/mean light supporting the sloped relation. An F-test following Kanbur & Ngeow (2004) furthermore demonstrates that the addition of the $\log P$ term in the PC relation makes a significant reduction in the error sum of squares term.

Again, $R^2 = 0$ for the Galactic bulge AC relations at mean light and $R^2 > 0$ at maximum/minimum light supporting the nature of relation obtained in the analysis. Similarly, for LMC AC relations also, $R^2 > 0$ at maximum/minimum light and $R^2 \approx 0$ at mean light as expected. The F-test shows that the addition of the amplitude term in the AC relation also significantly reduces the error sum of squares. The F statistic and corresponding $p(F)$, the probability of the F statistic for each PCAC relation are mentioned in Table 1.
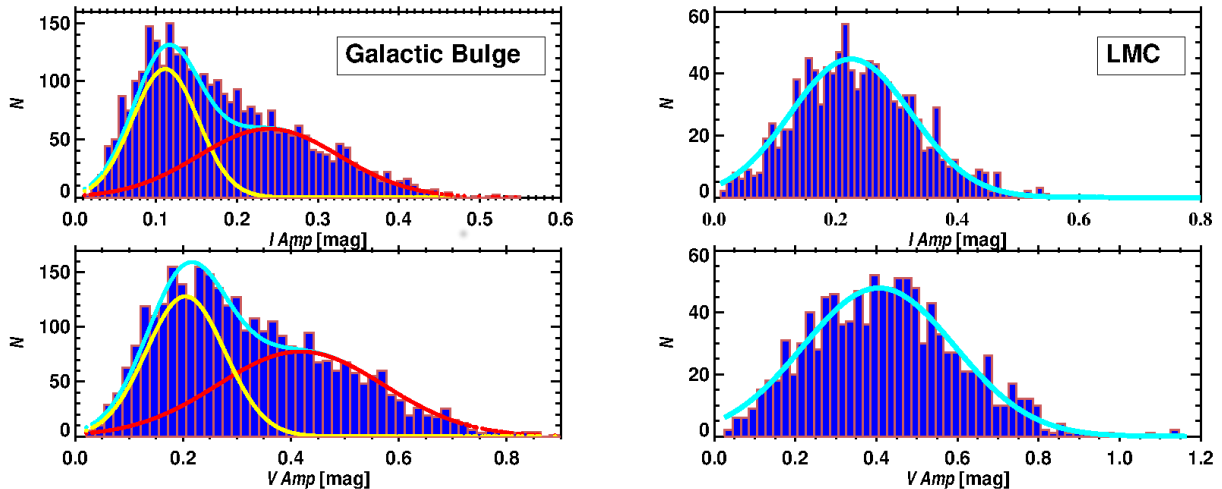
Figure 5. The left panel displays amplitude histograms for Galactic I (top figure) and V (bottom figure). The cyan lines denote a two-component Gaussian fit to both amplitude distributions. The individual Gaussian fits are given by yellow and red lines, respectively. For I-band, the fits are centred at 0.111 ± 0.002 (yellow-lower amplitude) and 0.240 ± 0.008 (red-higher amplitude). For the V-band, the corresponding values are centred at 0.204 ± 0.005 and 0.418 ± 0.024 for lower and higher amplitudes, respectively. The right panel presents the LMC amplitude histograms for I (top) and V (bottom) bands, respectively. The histogram is consistent with a single Gaussian fit (cyan) centred at 0.224 ± 0.003 and 0.406 ± 0.006 for the I- and V-band, respectively.
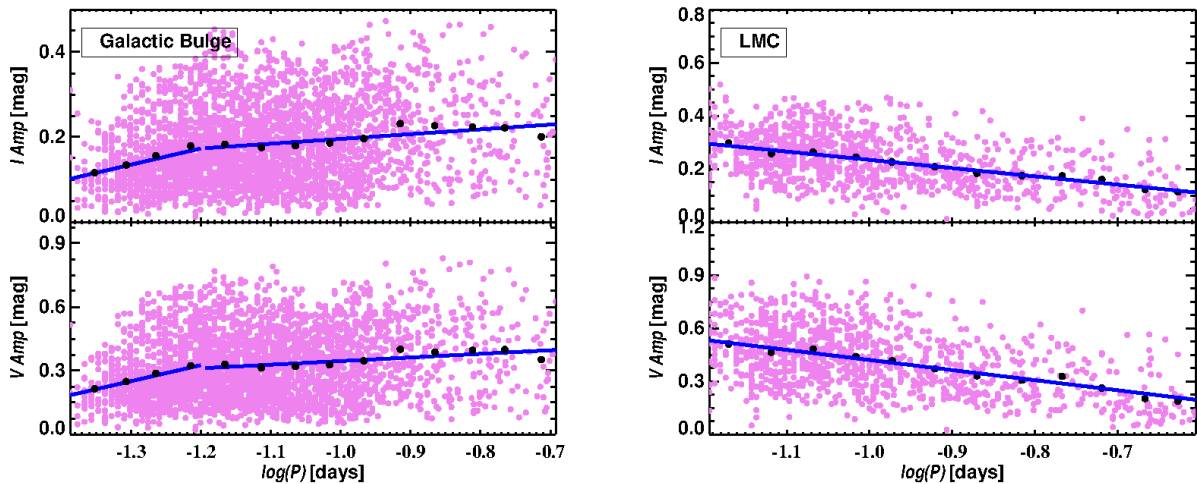
Figure 6. Left panel: PA diagram for Galactic bulge single mode δ Scuti stars (with iterative 3σ clipping). The blue lines represent the best-fit to the PA relations. There is a statistically significant break in the linear regression fit of Galactic bulge at $\log P = -1.2$. Binning of the data in every 0.05d in period (black dots) also shows the break in PA diagram at $\log P = -1.2$. Right panel: Same for LMC.

4.2 Period-Amplitude relation

The character of the PCAC relations displayed in Fig. 3 may be understood in part by looking at Fig. 4 which shows the histograms of the period and amplitude distribution. The left panel displays that the Galactic bulge δ Scuti stars are skewed towards shorter periods. The right panel implies that the LMC delta Scutis have higher amplitudes. Amplitude fluctuations are predominantly determined by temperature fluctuations. Thus, the lower/higher Galactic/LMC amplitudes are consistent with a flat/sloped PC relation at maximum light.

The left panel of Fig. 5 shows amplitude histograms for Galactic I (top figure) and V (bottom figure) bands. A two-component Gaussian

fit (cyan colour) to the amplitude distribution of Galactic bulge δ Scuti stars fits the data very well. This clearly indicates two populations of δ Scutis: one with lower amplitude (yellow colour) and another with higher amplitude (red colour). For I-band, the fits are centred at 0.111 ± 0.002 (yellow-lower amplitude) and 0.240 ± 0.008 (red-higher amplitude). For the V-band, the corresponding values are centred at 0.204 ± 0.005 and 0.418 ± 0.024, respectively. The right panel presents the LMC amplitude histograms for I (top) and V (bottom) bands, respectively. The histogram is consistent with a single Gaussian fit (cyan) centred at 0.224 ± 0.003 and 0.406 ± 0.006 for the I- and V-band, respectively. Hence, the LMC δ Scutis are of higher amplitudes and more evolved (Chang et al. 2013). From the intersection of the two Gaussians for the bulge, the lower/higher amplitude distribution
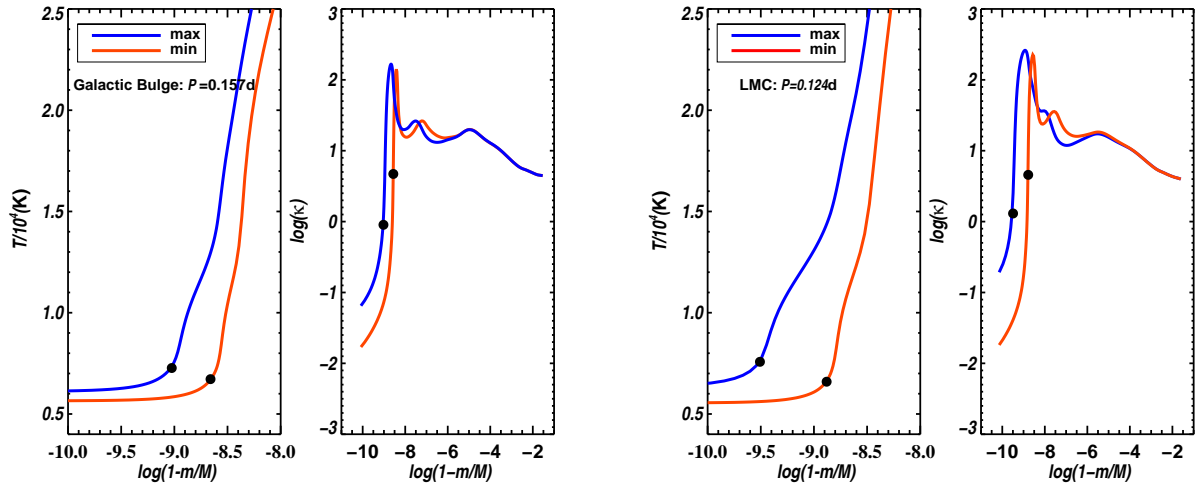
Figure 7. Theoretical temperature (left panel) and opacity profile (right panel) for a Galactic bulge (left figure) and LMC (right figure) δ Scuti star. The filled circles represent the location of the photosphere at $\tau = 2/3$.

dominates for *I*-band amplitude (*I* Amp) less/greater than 0.17 mag and *V*-band amplitude (*V* Amp) less/greater than 0.30 mag.

The OGLE-III LMC observed δ Scutis have mostly high amplitudes stars (Poleski et al. 2010). They did not include many (more than 1400) stars in their sample due to large photometric errors and/or small amplitudes. Hence, whilst the OGLE-IV Galactic δ Scuti sample may be complete, the OGLE-III LMC δ Scuti sample is likely to be missing a number of low amplitude stars. However, this provides an opportunity to compare a population of high amplitude δ Scutis in the LMC with a more mixed population in the Galactic bulge.

The δ Scuti PA plots for both Galaxy and LMC are given in Fig. 6, and the results are summarized in Table 2. It is found that the Galactic bulge PA relation exhibits a break at period 0.06 days, whereas no such break exists for the LMC δ Scuti stars. To test whether this break in the PA relation for the Galactic bulge δ Scutis is statistically significant, we use *F*-test (Kanbur & Ngeow 2004). From the *F*-test, the break in the PA relation at period 0.06 d is found to be statistically significant with an *F*-value equal to 8.662 and $p(F) \approx 0.0$. Further binning of the data (black dots) in every 0.05 d in period also supports the break in the PA relation at $\log P = -1.2$ as shown in Fig. 6.

For both the Galactic and LMC PA relations, $R^2 > 0$ supporting the sloped relation. The *F*-test also confirms that the addition of $\log P$ in the PA relation significantly reduces the error sum of squares.

The PA relations display contrasting behaviour: for Galactic/LMC stars, the amplitude increases/decreases with period. The period-colour relation indicates that Galactic δ Scuti stars are hotter than those in the LMC. Thus the Galactic blue edge δ Scuti instability strip is at a hotter temperature than that for the LMC. Thus, we have three regions: (i) the region mainly populated by Galactic δ Scutis and bordered by the Galactic blue edge and the LMC blue edge; (ii) the region populated by both Galactic and LMC δ Scutis bordered by the LMC blue edge and the Galactic red edge; (iii) the region mainly populated by LMC δ Scutis bordered by the Galactic red edge and the LMC red edge. As we go from region (i) to region (ii), the period and amplitude are increasing (the positive slope in the Galactic PA diagram); from region (ii) to region (iii), the period is increasing and the amplitude decreasing. This explains the negative slope in the LMC PA diagram. However, further investigation is required to verify this postulate.
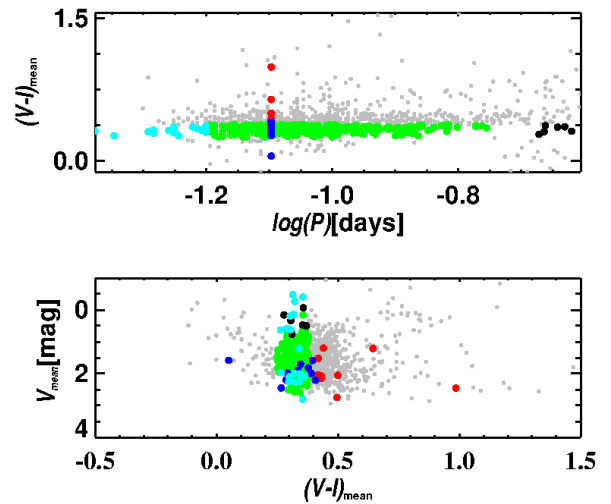

Figure 8. Upper panel: PC diagram for LMC δ Scuti stars at mean light. Lower panel: CMD for the same. The blue and red points indicate the hotter and cooler stars at a fixed period ($P \approx 0.08$ d), respectively. The green points indicate the stars of similar colour, while the cyan and black dots indicate the stars of shorter and longer period but of same temperature.

5 DISCUSSION

The large dispersion in the PC relations may be explained in part using PC and CMD diagrams (Fig. 8). In Fig. 8. We consider the data around a fixed period, say $P \approx 0.08$ *d*, and apply simple arguments based on the period-mean density theorem. Because the blue stars in Fig. 8 have a bluer colour, they are hotter and hence in order to have the same period, they need to have a higher L/M ratio. Meanwhile, the red stars have a redder colour. They are cooler and hence in order to have the same period, they need to have a lower L/M ratio. Thus, the blue and red stars on the PC diagram lie to the upper left and lower right, respectively, on a CMD diagram.

Now, if we choose stars covering a narrow range of colour on the PC plane - the green stars in Fig. 8. The black stars have longer period

but the same temperature and hence must have a higher L/M ratio, whilst the cyan stars have shorter period and the same temperature and hence must have a lower L/M ratio. We suggest that this can explain some of the dispersion seen in the PC plots. Another source of dispersion in the PC relations may also be due to the amplitude variations observed in some δ Scuti stars (Bowman et al. 2016).

5.1 A Possible Theoretical Explanation

The HIF and photosphere move in the mass distribution of the star and are not necessarily co-moving during a pulsation cycle. When the HIF and stellar photosphere are engaged (the stellar photosphere lies at the base of HIF), the temperature of the photosphere and hence the colour of the star are related to the temperature at which hydrogen ionizes. The temperature at which hydrogen ionizes is related to the properties of Saha ionization equilibrium: at low temperatures, the temperature at which hydrogen ionizes is largely independent of density and hence global stellar parameters. At higher temperatures, the temperature at which hydrogen ionizes is more dependent on the density and hence the stellar global parameters. Again, when the HIF and stellar photosphere are not engaged, then the photospheric temperature of the star has a stronger dependency on the stellar global parameters. As the colour is a measure of temperature and period is dependent on the stellar global parameters through the period-mean density relation, the relative location of HIF and photosphere at a particular pulsation phase will affect the corresponding PC relation (Das et al. 2020).

The changes in the PC relations at maximum/minimum light and the corresponding behaviour in the AC relations were explained by Simon, Kanbur & Mihalas (1993) by applying Stefan-Boltzmann law at maximum and minimum light using the following equation:

$$\log T_{\max} - \log T_{\min} = \frac{1}{10}(V_{\min} - V_{\max}), \tag{7}$$

where $T_{\max}$ and $T_{\min}$ denote the effective photospheric temperature at maximum and minimum light, respectively. Equation 7 indicates that if $T_{\max}$ is independent or more weakly dependent on the pulsation period, then the changes in amplitude are related to the temperature at minimum light, leading to a correlation between the V-band amplitude and the observed colour at minimum light. Conversely, if $T_{\min}$ is independent or weakly dependent on the period, then the V-band amplitude and the observed colour will be correlated at maximum light.

We have used the MESA-RSP version 'MESA r15140' (Paxton et al. 2010, 2013, 2015, 2018, 2019) which is based on the work of Smolec & Moskalik (2008) to compute two full-amplitude fundamental-mode models for δ Scuti stars with input parameters: $Z = 0.02$, $X = 0.70$, $M = 2.0\ M_\odot$, $L = 55\ L_\odot$, $T = 6950\ K$ (for Galactic bulge) and $Z = 0.008$, $X = 0.736$, $M = 1.6\ M_\odot$, $L = 25\ L_\odot$, $T = 6900\ K$ (for LMC). The model luminosities corresponding to the particular masses are consistent with the evolutionary track for δ Scuti stars. An example inlist used for computing the models is provided in Appendix A. Mass fractions of hydrogen and metals are taken from the literature (Bono et al. 1997; Templeton 2000). The Grevesse & Noels (1993) solar mixture is used to compute the models. The two models presented in this work are computed using convection parameter set A as outlined in Table 4 of Paxton et al. (2019). Detailed explanations of these free parameters can be found in Smolec & Moskalik (2008). For both models, the model envelope consists of $N = 200$ Lagrangian mass cells, with $N_{\text{outer}} = 60$ cells between the anchor and the surface. Thus, the HIF is always covered by a large number of zones throughout the pulsation cycle. The

criteria used to check whether the model has reached full amplitude pulsation cycle are: the pulsation period P computed on a cycle to cycle basis, the fractional growth of the kinetic energy per pulsation period Γ and the amplitude of radius variation ΔR should not vary by more than ~ 0.01 over the last $\sim 1000-$ cycles of the total integrations computed. As the growth rates of δ Scuti stars are very small, so it took ~ 22000 pulsation cycles for the Galactic model and ~ 54000 pulsation cycles for the LMC model to reach full amplitude stable pulsations for these models. Although MESA-RSP does not provide detailed atmosphere modelling and uses the diffusion approximation to determine the luminosity at different layers and bolometric corrections as a function of instantaneous temperature and effective gravity, previous work on PC relations for Cepheids and RR-Lyraes (Das et al. 2020, and references therein) has suggested that the diffusion approximation is adequate for the problems being discussed here.

Theoretical temperature and opacity profiles as function of mass distribution for each of the Galactic bulge and LMC models of δ Scuti stars are shown in Fig. 7. The temperature and the opacity profiles are obtained from the non-linear analysis using MESA-RSP (Paxton et al. 2019). The mass distribution is defined by the quantity $Q = \log\left(1 - \frac{m}{M}\right)$, where m is the mass within radius r and M is total mass. The photosphere is defined as the zone with an optical depth $\tau = \frac{2}{3}$. These models suggest that the HIF and photosphere are engaged throughout the pulsation cycle in a manner similar to that of RR Lyraes (Das et al. 2020).

For both the bulge and LMC theoretical models, at minimum light, the HIF and the photosphere are always engaged at a temperature regime for which the ionization of hydrogen is somewhat weakly dependent or independent of temperature and hence the period. This explains the observed small slopes of PC relations for both Galactic bulge and LMC δ Scuti stars at minimum light. On the other hand, the PC relation for the observed Galactic bulge δ Scuti stars at maximum light is flat, while that for the LMC, there is a significant slope. Although the HIF and stellar-photosphere are engaged for both Galactic bulge and LMC theoretical models (Fig. 7) at higher temperature, the observed bulge PC slope at maximum light is found to be close to zero. We note from these two non-linear models that the temperature of the photosphere at maximum light was higher for the LMC (~ 7576 K) than the Galactic (~ 7269 K). The temperatures at minimum light were comparable. This suggests that one manifestation of higher amplitudes is that the HIF is driven further out in the mass distribution at maximum light. Even though Galactic δ Scuti stars are hotter, their temperature fluctuations are smaller than their LMC counterparts leading to smaller amplitudes. These smaller amplitudes may be due to different locations of the instability strip in the Galaxy and LMC. The smaller Galactic δ Scuti amplitudes, caused by smaller temperature fluctuations lead to a flatter PC relation at maximum light. Hence, we have good support for the HIF stellar photosphere theory as described in Simon et al. 1993; Das et al. 2020, and references therein.

We also note that there is some controversy over the pulsation mode of δ Scuti stars and in fact whether they may be pulsating in a number of modes and/or have a non-radial component (Netzel et al. 2022; Lv et al. 2022; Khruslov 2022; Netzel & Smolec 2022). When we cross-checked our sample with the triple mode stars as listed in Netzel et al. (2022), we found 32 such stars in our sample. Removal of these stars from the sample does not affect the nature of the PCAC relations. Furthermore, whether a star is singly periodic or has some combination of radial and even non-radial modes, the net result is some periodic relative motion of the HIF and photosphere in the mass distribution. It is this net motion between the HIF and

photosphere that can determine the nature of the PC relation. The connection between PC and AC relations at two different phases does not contain any reference to mode of oscillation. Applying Stefan-Boltzmann's Law at maximum/minimum (Simon et al. 1993), we get $\frac{L_{\max}}{L_{\min}} \approx \frac{T_{\max}^4}{T_{\min}^4}$, or $\log L_{\max} - \log L_{\min} \approx \log T_{\max} - \log T_{\min}$, where $L_{\max}$ and $L_{\min}$ denote the maximum and minimum luminosity of a star, respectively and thereby determine the nature of the AC relation at minimum/maximum light depending on the behaviour of the PC relation at maximum/minimum light. In this case, a mixed population may indeed increase the dispersion of the PC or AC relation or lead to a different sloped relation. For example, first overtone RRc stars have a different sloped PC relation at minimum light as compared to fundamental mode RRab stars (Das et al. 2020, and references therein). However, the fundamental relation given above is still valid as long as temperature variations are the primary cause of luminosity variations. Thus, to some extent, the HIF-photosphere theory outlined above is independent of this discussion. All that matters is the relative position of the HIF and stellar photosphere.

Investigating the PC relations of δ Scuti stars restricted purely to one mode will be a future project. Das et al. (2020) computed theoretical PC relations for three classes of variable stars using two different formulations of time dependent convection (corresponding to parameter sets A and D in Paxton et al. (2019); Smolec & Moskalik (2008)). They found broad agreement between models and theory under all of A and D. In future work, we plan to construct larger grids of models and study in greater detail how these theoretical PC relations may vary with the parameter sets A,B,C,D.

6 SUMMARY AND CONCLUSIONS

In this work, the V and I-band light curves of δ Scuti stars belonging to the Galactic Bulge and LMC are utilized from the publicly available OGLE-IV and OGLE-III databases, respectively, to study the PCAC relations for these stars. These relations are obtained at maximum, mean and minimum light after applying iterative 3σ outliers removal and have been investigated for the first time using the largest available dataset. With this, we also extend the analysis of PCAC relation to much shorter periods ($\log P = -1.4$ d) which was done earlier down to $\log P = -0.5$ d (Fig. 8 of Das et al. 2020) adding δ Scuti stars to the classes of variable stars for which the HIF-stellar photosphere interaction theory has been successfully applied (Das et al. 2020). The results obtained in the present study are summarized as follows:

(i) The observed PCAC relations for δ Scuti stars in the bulge and LMC are consistent with the HIF-stellar photosphere theory as outlined in Das et al. (2020) and references therein.

(ii) The slopes of the PC relations for the Galactic bulge δ Scuti stars at maximum/mean/minimum light are flat and are statistically equal to zero. The AC relation is sloped at maximum/minimum light, while flat at mean light.

(iii) The PC relations for the LMC δ Scutis at maximum/mean light are sloped and flat at minimum light. The AC relations for LMC exhibit similar behaviour to that of the bulge, but the LMC AC relation has a relatively larger slope as compared to the bulge at maximum/minimum light.

(iv) The intercepts of PC relations at maximum/mean/minimum light of Galactic bulge stars have numerically smaller values as compared to those for the LMC stars. This indicates that the bulge δ Scutis are comparatively hotter than the LMC δ Scutis.

(v) Another important result obtained from this study is that the

LMC short period δ Scutis have larger amplitude as compared to the bulge.

(vi) Two populations of δ Scuti in the Galactic bulge are evident from their amplitude distributions: one with lower amplitude and another with higher amplitude. Because the LMC is located at a distance of roughly 50 kpc, many stars in the OGLE-III δ Scuti database were not included due to large photometric uncertainty in small amplitude measurements. Hence, OGLE-III LMC δ Scuti samples might have missed a number of small amplitude δ Scutis. Due to this observational bias, OGLE-III observed δ Scutis have mostly high amplitudes.

(vii) The PA relations are found to display contrasting behaviour: for Galactic/LMC stars, the amplitude increases/decreases with period. The period-colour relation shows that the Galactic blue edge δ Scuti instability strip is situated at a hotter temperature than that for the LMC. Considering three regions in the instability strip between the Galactic bulge blue edge and the LMC red edge, the observed positive/negative slope in the PA relation for Galactic bulge/LMC has been explained. However, further investigation is required to verify the underlying postulate which we are planning to do in a future paper.

DATA AVAILABILITY

The data underlying this article are available at http://ftp.astrouw.edu.pl/ogle/ogle4/OCVS/blg/dsct/ and http://ogle.astrouw.edu.pl/ for Galactic bulge and LMC, respectively. The derived data generated in this research will be shared on reasonable request to the corresponding authors.

REFERENCES

Beaton R. L., et al., 2016, ApJ, 832, 210
Bedding T. R., et al., 2020, Nature, 581, 147

Bhardwaj A., Kanbur S. M., Singh H. P., Ngeow C.-C., 2014, MNRAS, 445, 2655

Bhardwaj A., Kanbur S. M., Macri L. M., Singh H. P., Ngeow C.-C., Ishida E. E. O., 2016, MNRAS, 457, 1644

Bono G., Caputo F., Cassisi S., Castellani V., Marconi M., Stellingwerf R. F., 1997, The Astrophysical Journal, 477, 346

Bowman D. M., Kurtz D. W., Breger M., Murphy S. J., Holdsworth D. L., 2016, MNRAS, 460, 1970

Breger M., 1979, PASP, 91, 5

Breger M., Pamyatnykh A. A., 1998, A&A, 332, 958

Cardelli J. A., Clayton G. C., Mathis J. S., 1989, ApJ, 345, 245

Chang S. W., Protopapas P., Kim D. W., Byun Y. I., 2013, AJ, 145, 132

Das S., Bhardwaj A., Kanbur S. M., Singh H. P., Marconi M., 2018, MNRAS, 481, 2000

Das S., et al., 2020, MNRAS, 493, 29

Deb S., Singh H. P., 2009, AAP, 507, 1729

Gonzalez O. A., Rejkuba M., Zoccali M., Valenti E., Minniti D., Schultheis M., Tobar R., Chen B., 2012, A&A, 543, A13

Goupil M. J., Dupret M. A., Samadi R., Boehm T., Alecian E., Suarez J. C., Lebreton Y., Catala C., 2005, Journal of Astrophysics and Astronomy, 26, 249

Grevesse N., Noels A., 1993, Physica Scripta Volume T, 47, 133

Guzik J. A., 2021, Frontiers in Astronomy and Space Sciences, 8, 55

Haschke R., Grebel E. K., Duffau S., 2011, AJ, 141, 158

Jayasinghe T., et al., 2020, MNRAS, 493, 4186

Kanbur S. M., 1995, A&A, 297, L91

Kanbur S. M., Hendry M. A., 1996, A&A, 305, 1

Kanbur S. M., Ngeow C.-C., 2004, MNRAS, 350, 962

Khruslov A. V., 2022, Open Astronomy, 31, 148

Leys C., Ley C., Klein O., Bernard P., Licata L., 2013, Journal of Experimental Social Psychology, 49, 764

Lv C., Esamdin A., Pascual-Granado J., Yang T., Shen D., 2022, ApJ, 932, 42

Matsunaga N., et al., 2013, MNRAS, 429, 385

McNamara D., 1997, Publications of the Astronomical Society of the Pacific, 109, 1221

McNamara D. H., 2011, AJ, 142, 110

Murphy S. J., Hey D., Van Reeth T., Bedding T. R., 2019, MNRAS, 485, 2380

Nataf D. M., et al., 2013, ApJ, 769, 88

Nemec J. M., Balona L. A., Murphy S. J., Kinemuchi K., Jeon Y.-B., 2017, MNRAS, 466, 1290

Netzel H., Smolec R., 2022, Monthly Notices of the Royal Astronomical Society

Netzel H., Pietrukowicz P., Soszyński I., Wrona M., 2022, MNRAS, 510, 1748

Ngeow C.-C., Kanbur S. M., Bhardwaj A., Schrecengost Z., Singh H. P., 2017, ApJ, 834, 160

Nishiyama S., Tamura M., Hatano H., Kato D., Tanabé T., Sugitani K., Nagata T., 2009, ApJ, 696, 1407

Paxton B., Bildsten L., Dotter A., Herwig F., Lesaffre P., Timmes F., 2010, ApJS, 192, 3

Paxton B., et al., 2013, The Astrophysical Journal Supplement Series, 208, 4

Paxton B., et al., 2015, The Astrophysical Journal Supplement Series, 220, 15

Paxton B., et al., 2018, The Astrophysical Journal Supplement Series, 234, 34

Paxton B., et al., 2019, The Astrophysical Journal Supplement Series, 243, 10

Pietrukowicz P., et al., 2015, ApJ, 811, 113

Poleski R., et al., 2010, Acta Astron., 60, 1

Popowski P., 2000, ApJ, 528, L9

Poro A., et al., 2021, arXiv e-prints, p. arXiv:2102.10136

Riess A. G., et al., 2016, ApJ, 826, 56

Riess A. G., Casertano S., Yuan W., Macri L. M., Scolnic D., 2019, ApJ, 876, 85

Schlegel D. J., Finkbeiner D. P., Davis M., 1998, APJ, 500, 525

Simon N. R., Kanbur S. M., Mihalas D., 1993, ApJ, 414, 310

Skowron D. M., et al., 2021, ApJS, 252, 23

Smolec R., Moskalik P., 2008, Acta Astron., 58, 193

Soszyński I., et al., 2021, Acta Astron., 71, 189

Tammann G. A., Sandage A., Reindl B., 2003, A&A, 404, 423

Templeton M. R., 2000, PhD thesis, New Mexico State University

Udalski A., 2003, ApJ, 590, 284

Ziaali E., Bedding T. R., Murphy S. J., Van Reeth T., Hey D. R., 2019, MNRAS, 486, 4348

APPENDIX A: MESA INLIST

```
&star_job

    show_log_description_at_start = .false.

    create_RSP_model = .true.

    save_model_when_terminate = .true.
    save_model_filename = 'final.mod'

    initial_zfracs = 2

    color_num_files=2
    color_file_names(2)='blackbody_johnson.dat'
    color_num_colors(2)=5

    set_initial_age = .true.
    initial_age = 0

    set_initial_model_number = .true.
    initial_model_number = 0

    profile_starting_model = .true.
     set_initial_cumulative_energy_error = .true.
    new_cumulative_energy_error = 0d0

/ ! end of star_job namelist
&eos
    use_FreeEOS = .true.
/

&kap
    kap_file_prefix = 'gn93'
    kap_lowT_prefix = 'lowT_fa05_gn93'
    kap_CO_prefix = 'gn93_co'
    Zbase = 0.008

! opacity controls
    cubic_interpolation_in_X = .false.
    cubic_interpolation_in_Z = .false.
    include_electron_conduction = .true.
    use_Zbase_for_Type1 = .true.
    use_Type2_opacities = .true.
    kap_Type2_full_off_X  =  0.71d0
    kap_Type2_full_on_X   =  0.70d0
    kap_Type2_full_off_dZ  =  1d-3
    kap_Type2_full_on_dZ   =  1d-2

/
&controls
 ! must set mass, Teff, L, X, and Z.
        RSP_mass = 1.6 ! (Msun)
        RSP_Teff = 6900 ! (K)
        RSP_L = 25 ! (Lsun)
        RSP_X = 0.736 ! hydrogen mass fraction
        RSP_Z = 0.008 ! metals mass fraction

    RSP_alfa = 1.2d0   ! mixing length; alfa = 0 gives a purely radiative model.
    RSP_alfac = 1.0d0  ! convective flux; Lc ~ RSP_alfac
    RSP_alfas = 1.0d0  ! turbulent source; Lc ~ 1/ALFAS; PII ~ RSP_alfas
    RSP_alfad = 1.0d0  ! turbulent dissipation; damp ~ RSP_alfad
    RSP_alfap = 0.0d0  ! turbulent pressure; Pt ~ alfap
    RSP_alfap = 0.0d0  ! turbulent pressure; Pt ~ alfap
    RSP_alfat = 0.0d0  ! turbulent flux; Lt ~ RSP_alfat; overshooting.
    RSP_alfam = 0.25d0 ! eddy viscosity; Chi & Eq ~ RSP_alfam
    RSP_gammar = 0.0d0 ! radiative losses; dampR ~ RSP_gammar

    RSP_theta = 0.5d0  ! Pgas and Prad
    RSP_thetat = 0.5d0  ! Pturb
    RSP_thetae = 0.5d0  ! erad in terms using f_Edd
    RSP_thetaq = 1.0d0  ! avQ
    RSP_thetau = 1.0d0  ! Eq and Uq
    RSP_wtr = 0.6667d0  ! Lr
    RSP_wtc = 0.6667d0  ! Lc
    RSP_wtt = 0.6667d0  ! Lt
    RSP_gam = 1.0d0     ! Et src_snk

    ! controls for building the initial model
    RSP_nz = 200 ! total number of zones in initial model
    RSP_nz_outer = 60 ! number of zones in outer region of initial model
    RSP_T_anchor = 11d3 ! approx temperature at base of outer region
    RSP_T_inner = 2d6 ! T at inner boundary of initial model

    RSP_max_outer_dm_tries = 100 ! give up if fail to find outer dm in this many attempts
    RSP_max_inner_scale_tries = 100 ! give up if fail to find inner dm scale factor in this many attempts
    RSP_T_anchor_tolerance = 1d-8
    RSP_relax_initial_model = .true.
    RSP_relax_alfap_before_alfat = .true. ! else reverse the order
    RSP_relax_max_tries = 1000
    RSP_relax_dm_tolerance = 1d-6
    use_RSP_new_start_scheme = .false.
    RSP_kick_vsurf_km_per_sec = 1.0d0
    RSP_fraction_1st_overtone = 0.1d0
    RSP_fraction_2nd_overtone = 0d0

    ! random initial velocity profile.  added to any kick from eigenvector.
    RSP_Avel = 0d0 ! kms. linear in mesh points from 0 at inner boundary to this at surface
    RSP_Arnd = 0d0 ! kms. random fluctuation at each mesh point.

    ! period controls
    RSP_target_steps_per_cycle = 600
    RSP_min_PERIOD_div_PERIODLIN = 0.5d0
    RSP_mode_for_setting_PERIODLIN = 0
    RSP_default_PERIODLIN = 34560

    ! when to stop
    RSP_max_num_periods =54000 ! ignore if < 0

    RSP_GREKM_avg_abs_frac_new = 0.1d0 ! fraction of new for updating avg at each cycle.
    ! timestep limiting
    RSP_initial_dt_factor = 1d-2 ! set initial timestep to this times linear period/target_steps_per_cycle
    RSP_v_div_cs_threshold_for_dt_limit = 0.8d0

    RSP_max_dt_times_min_dr_div_cs = 2d0 ! limit dt by this
    RSP_max_dt = -1 ! seconds
    RSP_report_limit_dt = .false.
    RSP_cq = 4.0d0 ! viscosity parameter (viscosity pressure proportional to cq)
    RSP_zsh = 0.1d0 ! "turn-on" compression in units of sound speed.
    RSP_Qvisc_linear = 0d0
    RSP_Qvisc_quadratic = 0d0
    RSP_use_Prad_for_Psurf = .false.
    RSP_use_atm_grey_with_kap_for_Psurf = .false.
    RSP_tau_surf_for_atm_grey_with_kap = 3d-3 ! for atm_grey_with_kap
    RSP_fixed_Psurf = .true.
    RSP_Psurf = 0d0 ! ignore if < 0.  else use as surface pressure.

    ! solver controls
    RSP_tol_max_corr = 1d-8
    RSP_tol_max_resid = 1d-6
    RSP_max_iters_per_try = 100
    RSP_max_retries_per_step = 8
    RSP_report_undercorrections = .false.
    RSP_nz_div_IBOTOM = 30d0 ! set IBOTOM = RSP_nz/RSP_nz_div_IBOTOM
    RSP_min_tau_for_turbulent_flux = 2d2
    ! rsp hooks
    use_other_RSP_linear_analysis = .false.
    use_other_RSP_build_model = .false.

    RSP_efl0 = 1.0d2
    RSP_nmodes = 3
    RSP_trace_RSP_build_model = .false.

! output controls

    num_trace_history_values = 3
    trace_history_value_name(1) = 'rel_E_err'
    trace_history_value_name(2) = 'log_rel_run_E_err'
    trace_history_value_name(3) = 'rsp_GREKM_avg_abs'

    photo_interval = 1000
    profile_interval = 1
    history_interval = 1
    terminal_interval = 4000
    max_num_profile_models = -1
    log_directory='LOGS'
    photo_directory='photos'
/ ! end of controls namelist
&pgstar
/ ! end of pgstar namelist
```

This paper has been typeset from a TEX/LATEX file prepared by the author.